AN ELECTROGRAPH FOR MEASUREMENT OF MACROSCOPIC ELECTRIC FIELDS IN PROMINENCES AND FLARES

T. MORAN and P. FOUKAL

Cambridge Research and Instrumentation, Inc., Cambridge, MA 02139, U.S.A.

(Received 25 February, 1991)

Abstract. We describe an 'electrograph' instrument designed for measurement of macroscopic electric fields in solar plasmas, using the polarization dependence of line width in Stark-broadened hydrogen Paschen emission lines. Observations of quiescent prominences and limb chromosphere with our electrograph at the NSO/Sac Peak Evans Coronal Facility provide upper limits of 5–10 V cm^{-1} for transverse macroscopic electric fields in these structures, averaged over an area of about 5 × 7 arc sec. Random thermal motions of hydrogen ions across magnetic field lines generate a quasi-static electric field, which should be distinguishable from pressure broadening in the intensely magnetized chromosphere over a sunspot, given an electrograph sensitivity a factor 2–3 better than that achieved here. Future electrograph measurements of limb flares, post-flare loops and eruptive prominences, even at 5 V cm^{-1} sensitivity, could provide a useful new test of reconnection and discharge effects in such dynamic structures.

1. Introduction

The first observation of solar magnetic fields was achieved by G. Hale in 1908, using the Zeeman effect observed in sunspots. Soon afterward, A. Wien drew attention to the possibility of detecting accompanying motional ($\mathbf{v} \times \mathbf{B}$) electric fields in sunspots, in his classic paper on the first measurement of such motional fields in the laboratory using the Stark effect (Wien, 1916).

Surprisingly little attention has been devoted to the investigation of possible macroscopic electric fields in the solar atmosphere considering the important role that quasi-static and wave-related electric fields play in models of dynamic solar phenomena. Foukal and Hinata (1991) have reviewed the observations and some of the sources of possibly observable fields in flares, post-flare loops and eruptive prominences. Measurements are required to determine the detectability of the emission measures and time scales of the electrified plasmas expected from models of such structures.

In this paper we describe an instrument designed to measure the intensity and orientation of the macroscopic electric field component transverse to the line of sight. Our technique makes use of the polarization structure of hydrogen lines Stark-broadened by a quasi-static electric field. A similar technique was used previously in flare observations on the disc in Hα (Dravins, 1973) and was introduced independently in observations of post-flare loops at the limb by Foukal, Hoyt, and Gilliam (1986). This approach has also been used in laboratory plasma research to study turbulent electric fields in *Z*-pinch machines (Berezin, Dubovoi, and Lyublin, 1972a, b), and more recently to study the magnetic field structure in tokamaks using the motional electric field in a diagnostic beam of neutral hydrogen (Levinton *et al.*, 1990).

In Section 2 and 3 we describe the basic technique and the instrument. In Section 4

Solar Physics **135:** 179–191, 1991.

we describe our observations of quiescent prominences and of the limb chromosphere. In Section 5 we explain how the $\mathbf{v} \times \mathbf{B}$ electric fields expected due to random thermal motions of hydrogen in a uniformly magnetized atmosphere should provide a minimum detectable macroscopic electric field. We summarize our results and discuss plans for future work in Section 6.

2. The Electrograph Technique

The technique described in this paper relies on the strong linear Stark-effect in hydrogen (see, e.g., Bethe and Salpeter, 1957). While energy levels in all atoms and ions undergo quadratic Stark shifts in electric fields, only energy levels in hydrogen and hydrogen-like ions experience linear (first-order) Stark shifts. This is due to the l-degeneracy in hydrogen and hydrogen-like ions, which is a consequence of the angular invariance of their Hamiltonian. The first-order Stark shifts in these species are at least a factor of 100 greater than the quadratic shifts at the field strengths we expect (< 1000 V cm^{-1}).

First-order Stark shifts in hydrogen and hydrogen-like species may be obtained by solving the unperturbed Schrödinger equation in a parabolic coordinate system for the unperturbed eigenstates and energies, and computing the expectation value of the electric field interaction operator. The electric field interaction is included as a perturbation. The spin-orbit interaction term is ignored in the perturbation analysis (the 'strong' field limit) and added to the computed energy shift as a correction. Solution of the equation in parabolic coordinates is convenient, since the Stark shifts are expressed simply in terms of the parabolic quantum numbers n_1 and n_2, and of the principal quantum number n. Here n is equivalent to the principal quantum number characterizing the spherical hydrogen or hydrogen-like states. The parabolic quantum numbers n_1 and n_2 have integer values ranging from 0 to $n - 1$. The difference, $n_1 - n_2$, is an indicator of the asymmetry, or charge separation, of the state.

The energy shift, ΔU, of level n, n_1, n_2, is given by

$$\Delta U = 3/2n(n_1 - n_2)E/Z^2 , \tag{1}$$

where Z is the nuclear charge and E is the electric field strength, all in atomic units. With $Z = 1$, hydrogen has the largest linear Stark shift of any hydrogen-like species.

The number of sublevels is $2n - 1$. The wavelength shift of the line component for the transitions between the states n, n_1, n_2, m, and n', n_1', n_2', m' in hydrogen is given by

$$\Delta\lambda = 6.42 \times 10^{-5} \lambda^2 (n(n_1 - n_2) - n'(n_1' - n_2'))E , \tag{2}$$

with λ in cm and E in V cm^{-1}. Components with $\Delta m = 0$ (π components) are linearly polarized parallel to the electric field direction, while components with $\Delta m = \pm 1$ (σ-components) are linearly polarized perpendicular to the field direction. When the emitted radiation is viewed in a direction along the electric field, the wavelength shifts corresponding to the σ-components will be seen, and no net polarization is measured.

From Equation (2), we can see that measurements of lines of high-n and low-n'

provide the best sensitivity to E. Since for the high-n lines measured for this study the upper value of n exceeds the lower by at least a factor of four, the electric field wavelength splitting $\Delta\lambda$ is determined almost entirely by the upper level n. The mean value of $n_1 - n_2$ is proportional to n, from which it follows that the mean energy splitting, and therefore the mean wavelength splitting, is proportional to n^2, i.e.,

$$\Delta\lambda \sim \lambda^2 n^2 E\,. \tag{3}$$

The mean electric field splitting therefore increases quadratically with upper quantum number as well as with wavelength.

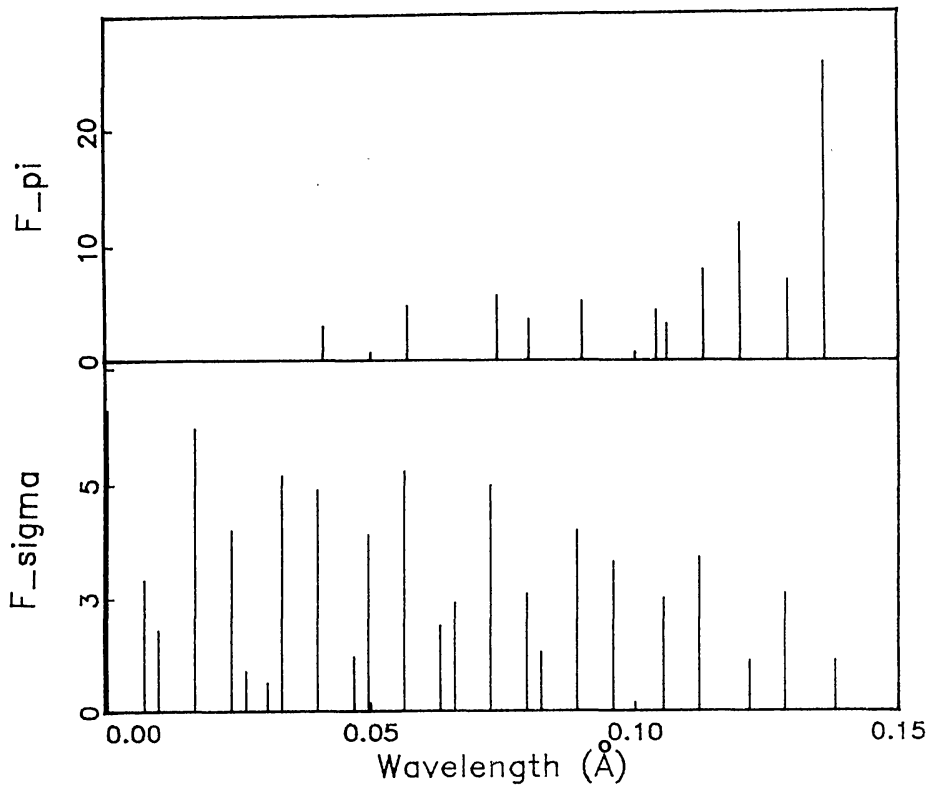

Fig. 1. Plots showing the π (*upper panel*) and σ (*lower panel*) oscillator strengths of the P18 line versus wavelength shift for a 10 V cm^{-1} field. Shifts and oscillator strengths have been taken from Underhill and Waddell (1959). The plot shown represents one half of the full pattern, which is symmetric about the origin.

Figure 1 shows a plot of the oscillator strengths of the π- and σ-components of the Paschen 18 (P18) line ($n = 18 \rightarrow n = 3$) in the presence of a 10 V cm^{-1} electric field transverse to the line of sight. Fine structure splitting, which would introduce wavelength shifts of 30 mÅ (mean value) is ignored for simplicity, since the full width of the pattern shown here exceeds 250 mÅ. The plot shows that the π-components have a greater mean wavelength shift than the σ-components. Our technique for the detection of macroscopic electric fields relies on this difference in the magnitude of the mean σ- and π-Stark shifts.

In the coronal structures we observe, magnetic fields are of order 100 G or less, so Zeeman broadening of the hydrogen lines of interest is negligible (< 10 mÅ). Doppler broadening, plasma pressure broadening (which produces randomly-directed electrostatic fields) and broadening by longitudinal macroscopic electric fields, are unpolarized. Only broadening by a macroscopic electric field transverse to the line of sight would depend on polarization. The n^2 dependence of Stark splitting also distinguishes macroscopic or pressure broadening from Doppler broadening which varies as λ. Furthermore, any variations of broadening caused by macroscopic fields would increase with n, though not in strict proportion to n^2, since the broadening contributions add quadratically.

Since the macroscopic broadening depends quadratically on wavelength and upper quantum number we measure the highest-n observable Paschen series lines which have wavelengths around 8500 Å, rather than the (brighter) high lines of the Balmer series, which have wavelengths around 3700 Å. We study these lines in emission above the limb to achieve highest signal-to-noise ratio in the line profiles, although disc observations in flares are also possible.

Our technique involves measurement of a high-n Paschen emission line profile at a series of settings of a polarization analyzer, which selects the plane of linear polarization admitted to the spectrometer. The amplitude of variation in the line half-widths is determined by the magnitude of the macroscopic electric field transverse to the line of sight. The direction of the polarization analyser transmission axis at maximum broadening corresponds to the direction of the electric field axis projected on the plane of the skey. Opposite field directions produce identical spectra, so this technique determines the direction of the electric field to within a 180° rotation.

Most of our observations have been carried out on P18, the highest Paschen line for which the π- and σ-components have been tabulated by Underhill and Waddell (1959). Figure 2 shows the calculated P18 π- and σ-components in a 10 V cm^{-1} field. They have been convolved with a gaussian of 0.5 Å FWHM, which is the minimum thermal broadening we have observed for this line in prominences. The difference in halfwidth between the profiles in the two polarizations is 0.043 Å. The P18 line widths observed in solar prominences typically range between 0.5 and 0.8 Å.

Figure 3 shows a plot of the difference (modulation) in halfwidth between the π- and σ-polarizations of the P18 line as a function of electric field strength, for a line of total FWHM 0.8 Å. The fine structure splitting, which is proportional to n^{-3}, has been added to lower levels as a correction. The width modulation increases as the square of the electric field strength at low field strengths. A Taylor series expansion of the halfwidth in the field strength shows a quadratic dependence of halfwidth on field strength at low fields, since the various contributions to line broadening add quadratically and the macroscopic electric field broadening at these field strengths is small compared to the polarization-independent broadening contributions. At higher fields, the modulation becomes linear with field strength.

In addition to polarization effects on the halfwidth, the line shape itself could in principle be used to discriminate between broadening by a uniform macroscopic field,

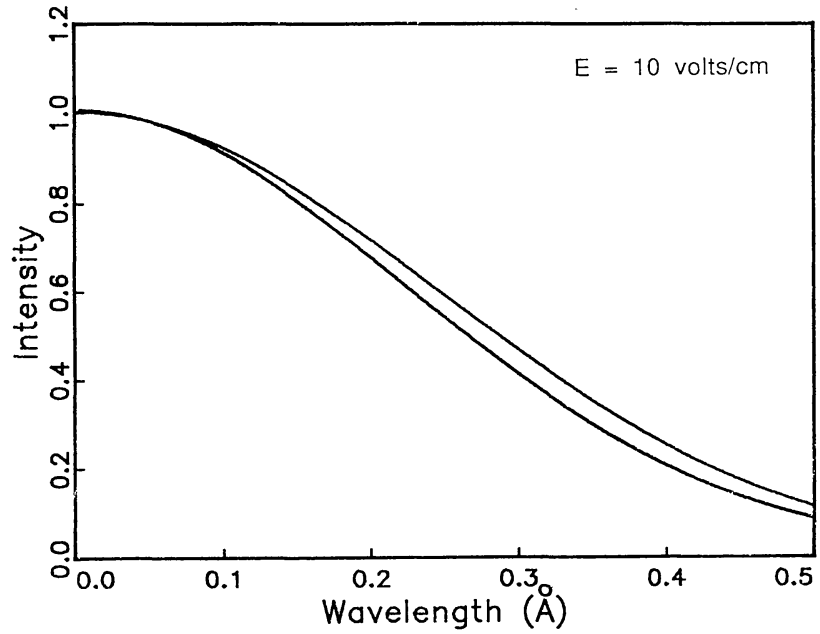

Fig. 2. Plots of the π (upper curve) and σ (lower curve) components for P18 in a 10 V cm^{-1} field, convolved with a gaussian of 0.5 Å FWHM. The difference in halfwidth between the two profiles is 0.043 Å.

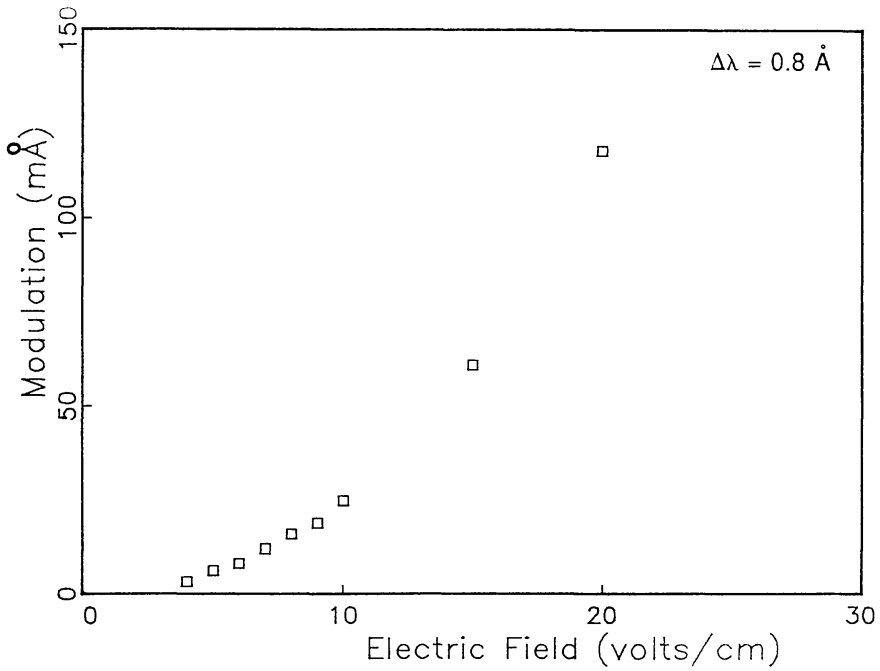

Fig. 3. A plot of the difference in halfwidth (modulation) between the π and σ P18 profiles as a function of electric field strength for a line of 0.8 Å FWHM.

and by pressure-broadening. In pressure-broadening the probability that an atom feels an electric field of strength E is given by the Holtzmark distribution function, which has a maximum near the 'normal' field strength (see, e.g., Griem, 1974), although it has a significant tail, which raises the 'mean' electric field to about 3 times the normal field.

The effect of the large electric fields in the tail of the distribution is to enhance the hydrogen line wings in a pressure-broadened line relative to the macroscopic broadening case. This distinction could be made, if the wing shape is measured to sufficient accuracy.

3. Instrumentation

The instrument (electrograph) which we have constructed consists of a near-infrared polarization analyzer and a PC-controlled Pulnix TM840N integrating CCD camera. The polarization analyzer is made up of an achromatic (for wavelengths between approximately 8000 and 9000 Å) half-waveplate rotated by a PC-controlled stepping motor, followed by an infrared polarizer mounted at a fixed angle. The analyzer is located directly behind the occulting disk of the 40 cm coronagraph at the Sacramento Peak Evans Coronal Facility (Figure 4). The CCD is positioned at the exit focus of the Evans Facility universal spectrograph (USG) and records Paschen line spectra in first order.

The CCD camera contains a windowless (to avoid fringes) Sanyo chip (800h × 480v) with high quantum efficiency ($>30\%$) at the wavelengths of interest. This chip spans 32 Å at the 5 Å mm^{-1} first-order dispersion of the USG. A 45 μm slit yields a wavelength resolution of 0.25 Å and a projected slit width on the Sun of 0.86 arc sec. The chip is cooled by a Peltier device in thermal contact with the back side of the chip. Dry ice is applied to the cooler's heat sink, bringing the chip temperature to $-30\,^{\circ}C$. The resulting low dark count levels make 60 s exposures possible. Our tests on prominences have shown that the CCD-based system is a factor of 20 more sensitive than IR-sensitive film at these wavelengths. Recent tests have also shown that the read-out noise can be significantly reduced through use of a slow-scanned CCD, and we plan to substitute such a camera for the Pulnix in the near future.

The camera is controlled through a Data Translation 2853 frame grabber board installed in a Compaq 286 PC (12 MHz, 40 megabyte hard disk). Control software sets the camera exposure and averages a specified row section on the chip to obtain the spectrum. The stepper motor is controlled through a driver board installed in the Compaq. In data collection the waveplate is rotated in 30 degree steps and the CCD exposes a frame at each angular location. The spectra are stored on the PC's hard disk. A menu-driven master program simultaneously controls the camera exposure, stepper motor, data collection, and data storage. The halfwidths are calculated in software from the smoothed profiles.

4. Observations and Results

Electrograph observations were obtained during five observing runs between May 1989 and November 1990. No limb-flares or post-flare loops occurred during these runs, but observations of seven quiescent prominences and the chromosphere were carried out. Plots of four representative Paschen line emission profiles between P11 and P21,

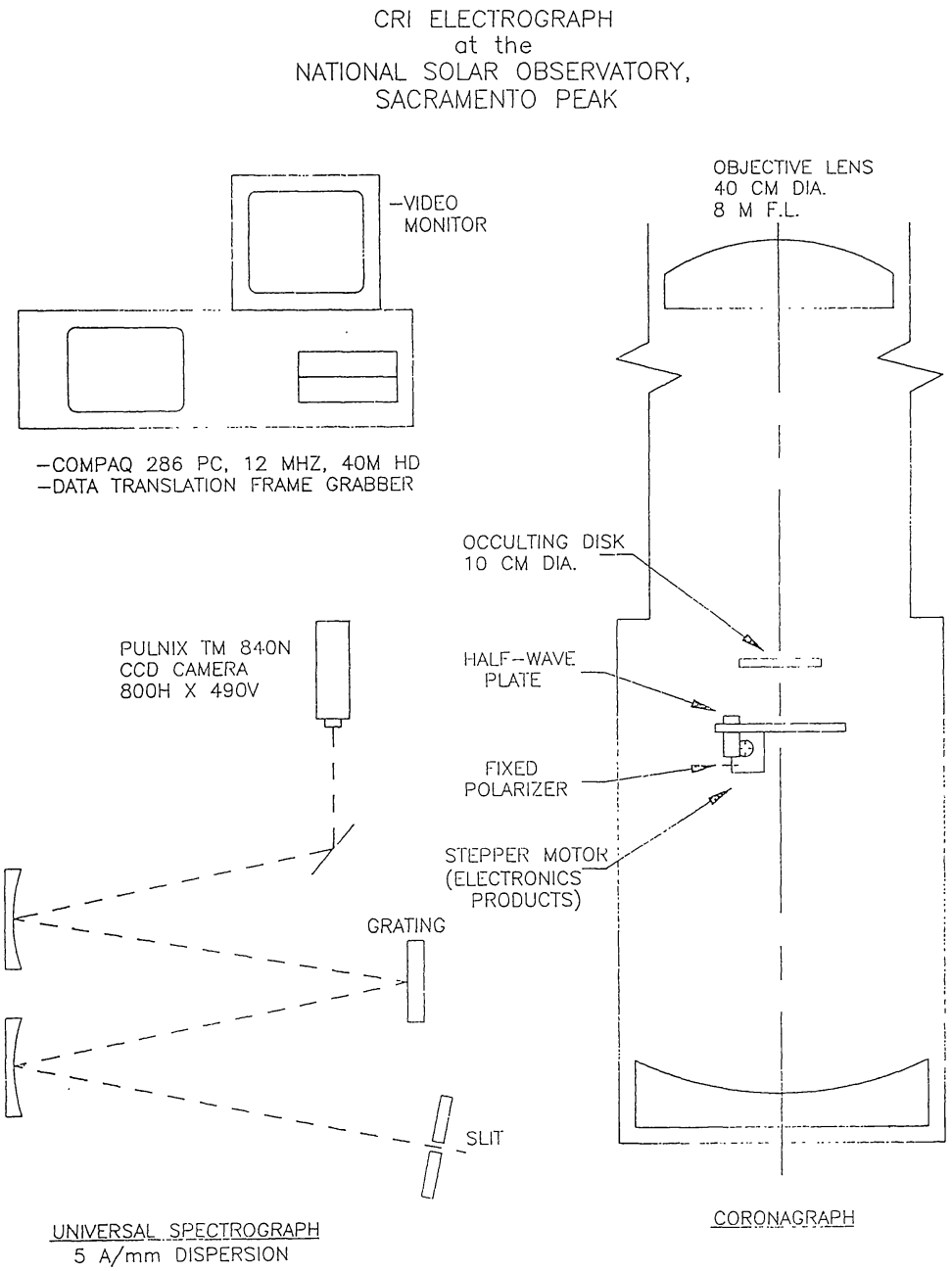

Fig. 4. A schematic diagram of the CRI electrograph installed on the 40 cm coronagraph and Universal Spectrograph at the SPO Evans Facility.

observed in a quiescent prominence on November 10, 1990, are shown in Figure 5. Each of these plots represents a sum of 12 spectra, acquired at 30° steps in half-wave plate orientation, to obtain an angle-averaged spectrum. The spectra were smoothed using a 70 mÅ gaussian filter which added less than 1 mÅ to the typical line width of 0.7 Å. Exposure times varied from 2 s for P9 to 40 s for P20.

Figure 6 shows plots of angle-averaged Paschen line halfwidths for two prominences and for the chromosphere. The noise in the prominence halfwidths shown here is due primarily to variations in line shape caused by the superposed Fraunhofer and telluric

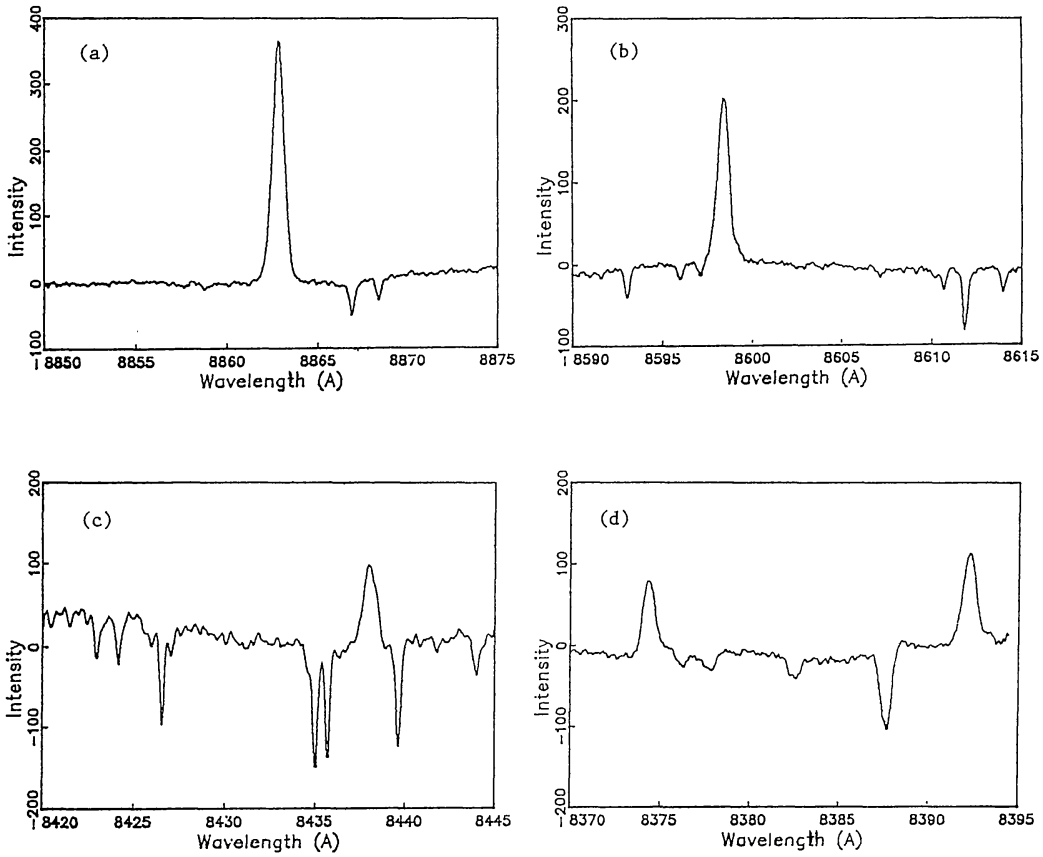

Fig. 5. A plot of the (a) P11, (b) P14, (c) P18, (d) P20 and P21 emission lines in a quiescent prominence.

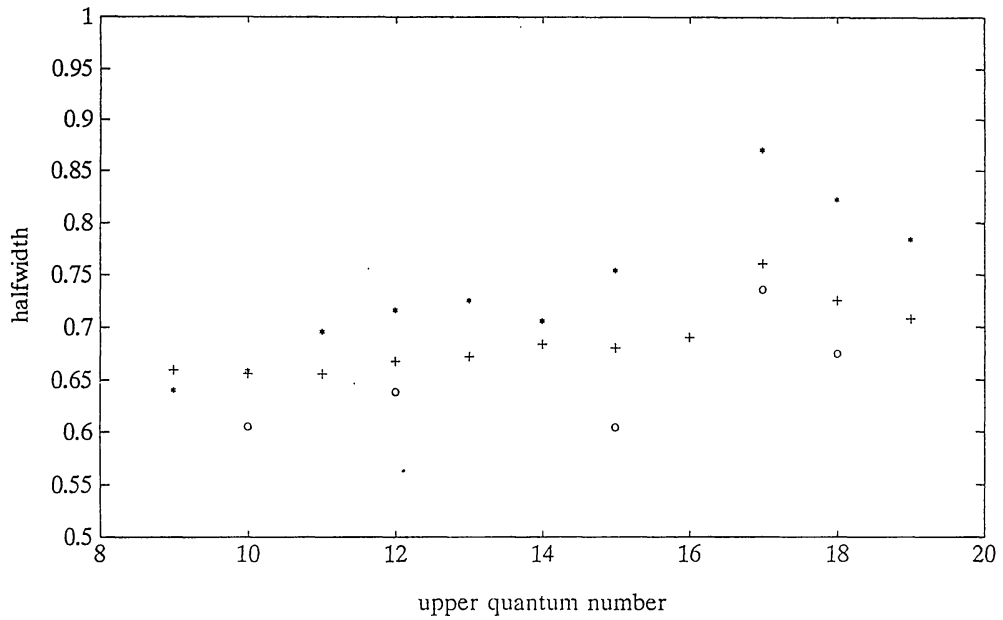

Fig. 6. Plots of angle-averaged Paschen line half-widths vs n for prominences observed on November 10, (*), November 11, 1990, (+); and for the chromosphere (○).

absorption lines scattered onto the emission spectrum, as seen in Figure 5. Some of the noise in the chromospheric line widths is due to variations in pointing caused by seeing, which changes the viewing height and thus the line profile in the steep radial gradient of chromospheric intensity. The general increase of angle-averaged halfwidth with n seen in Figure 6 indicates Stark-broadening in these optically thin lines, since the Doppler contribution to broadening decreases by about 9% between 9229 Å (n = 9) and 8392 Å (n = 20).

The main data produced by the electrograph consist of plots of P18 halfwidth against polarization angle. Results for two prominences observed on November 10–11, and for a prominence observed on April 21, 1990, are shown in Figure 7 along with a similar plot for the limb chromosphere observed on November 13. Note that only differences in the width of a given line, measured at various orientations of the input plane of linear polarization, contribute to the signal. Thus, distortions of the line shape caused by coincidences with scattered Fraunhofer absorption lines (or blending with emission lines of metals) should contribute little noise to the electrograph output. The uncertainty in variation of the P18 line width is determined here by chip read-out electronics and digitization. Typical signal-to-noise ratios are 100–400 for sums of 2–4 spectra. This leads to uncertainties of 0.3–1.2% in variation of the P18 halfwidth, and to an electric field sensitivity of 5–10 V cm^{-1}.

None of the P18 line widths shown in Figure 7 exhibit any significant modulation beyond the noise limits of 7–10 mÅ. Thus, our observations yield an upper limit for macroscopic electric field strength of 5–10 V cm^{-1} in these prominences and chromosphere. This limit applies to a spatial average given (in the direction of spectral dispersion) by the seeing and guiding accuracy of roughly 5 arc sec during an electrograph

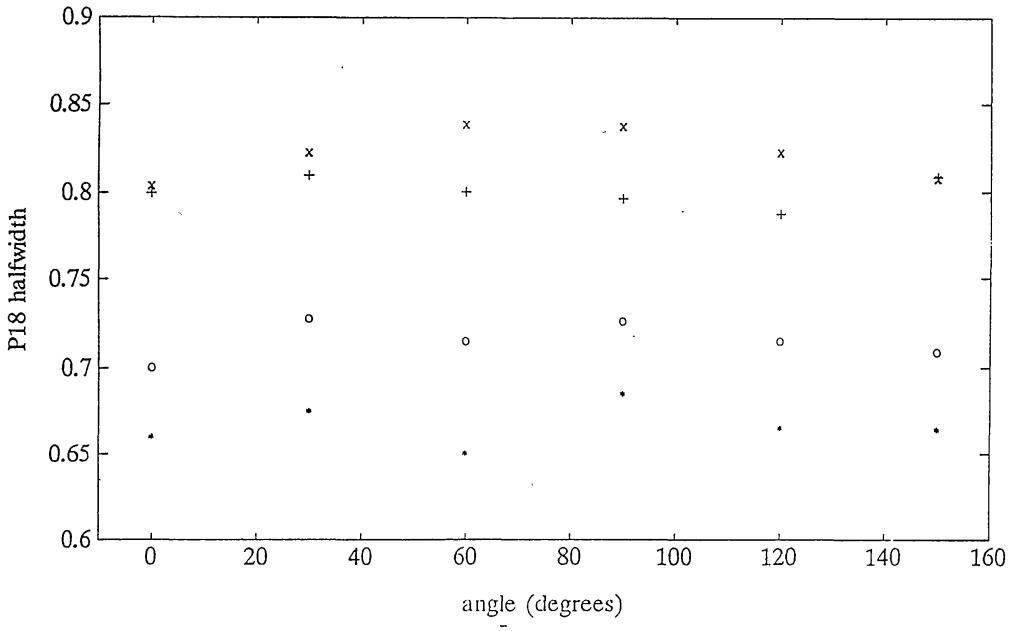

Fig. 7. Plots of P18 halfwidth vs polarization angle for prominences observed on April 21 (+), November 10 (×) and November 11 (○), and for the chromosphere (*).

duty cycle lasting between 5 and 10 min. Along the slit, the averaging of CCD rows extends over about 7 arc sec on the Sun. Thus, the upper limit obtained here averages over an area of roughly 35 (arc sec)^2.

5. Motional Stark Effect as a Magnetic Field Diagnostic in Thermal Plasmas

In principle, the electric field limits obtained above might also provide upper limits for magnetic field strengths in these prominence and chromospheric plasmas, since an atom moving at thermal velocity in a magnetic field experiences a motional electric field in its reference frame. The mean absolute values of the x, y, and z-components of the motional electric field felt by a Maxwellian distribution of hydrogen atoms are calculated in the Appendix. If the line of sight coincides with the z-axis and the magnetic field has components along z and x (Figure A1), the mean absolute electric field components are given by

$$\overline{E}_x = 7.3 \times 10^{-5} \sqrt{T}\, |B_z| \,, \tag{4}$$

$$\overline{E}_y = 3.7 \times 10^{-5} \sqrt{T}\, (|B_\perp - B_z| + |B_\perp + B_z|) \,, \tag{5}$$

and

$$\overline{E}_z = 7.3 \times 10^{-5} \sqrt{T}\, |B_\perp| \,, \tag{6}$$

where B_z and $B_\perp$ (gauss) are the z- and x-components of magnetic field, T is the ion temperature, and the electric fields are expressed in V cm^{-1}.

For a magnetic field directed purely along the line of sight, the motional electric fields lie in the x, y (transverse) plane, and the mean x and y field strengths will be equivalent, since Equation (5) reduces to Equation (4). Thus there will be no variation of line broadening with half-waveplate angle. In this case, contributions from the σ and π Stark-components could not be distinguished from pressure broadening.

If the magnetic field lies transverse to the line of sight (e.g., along the x-axis) the motional electric fields will lie in the y, z-plane. In this case Equation (5) reduces to Equation (6) and mean values of the motional electric fields along y and z are equivalent. The electric fields along z give rise to an angle-independent line broadening which is equivalent to the σ broadening in the transverse field case. But the motional electric fields along y would be detectable as a polarization-dependent broadening determined by the mean field strength.

The mean motional electric field strength felt by the hydrogen atoms in the prominences and chromospheric region observed, obtained from Equation (6), is approximately $7 \times 10^{-3} B_\perp$ V cm^{-1}, taking $T \cong 9 \times 10^3$ K. Therefore, our transverse macroscopic field limits of 5 V cm^{-1} for the prominences and for the chromosphere yield upper limits of roughly 500 G for transverse magnetic fields in these objects. These values are two orders of magnitude higher than magnetic field intensities measured in quiescent prominences (see, e.g., review by Hirayama, 1985). However, the technique might be applied in the chromosphere over umbrae, since fields exceeding 1 kG have

been reported in the sunspot transition region (Henze *et al.*, 1982) and in the sunspot corona (White, Kundu, and Gopalswamy, 1991), and the field geometry should be essentially transverse when a spot is observed near the limb.

6. Summary and Discussion

The upper limits of even 5 V cm^{-1} derived above considerably exceed estimates of electric field intensities expected in quiescent prominences from processes such as quasi-static Joule heating or neutral sheet dissipation (see review by Foukal and Hinata, 1991). Thus it is not surprising that macroscopic fields were not detected in our observations of such structures. The motional ($\mathbf{v} \times \mathbf{B}$) electric field expected in uniformly magnetized thermal plasmas provides a minimum field value that should be detectable in the chromosphere over sunspots, so observation of large spots near the limb could provide a relatively model-independent test of the electrograph sensitivity. Replacement of our present CCD with a slow-scanned camera should help to detect such fields by further reducing our electronic read-out noise to the 1 V cm^{-1} level.

But even the sensitivity of 5 V cm^{-1} achieved here is well within the range of quasi-static electric field intensities (both perpendicular and parallel to B) expected from models of such flare-associated processes as electric discharges, return currents, and neutral sheet reconnection (see discussion by Foukal and Hinata, 1991). As discussed in that review, sensitivity at that level should also be sufficient to detect both Alfvén and plasma waves associated with dynamic events, when their electric vector lies in the sky plane. The emission measures in H I and time scales of these phenomena are still quite uncertain. Future electrograph observations of flares, post-flare loops and eruptive prominences should be of great interest in determining whether electric field measurements can be exploited to provide new insights into magnetic energy dissipation and particle acceleration in these structures.

Acknowledgements

We thank Heinz Kochling and Ruel Little for assistance in the design and construction of the electrograph. We are also grateful to Lou Gilliam, Brian Armstrong and Joe Elrod for observing assistance at the Evans Coronal Facility at Sacramento Peak. This work has been supported under Air Force SBIR contract F19628–87–C–0110 and NASA contract NASW-4538.

Appendix. Calculation of Mean Motional Electric Fields in a Uniformly Magnetized Thermal Hydrogen Plasma

An atom moving in a magnetic field will experience a motional ($\mathbf{v} \times \mathbf{B}$) electric field. In order to calculate the mean absolute value of this field experienced by an atom in a Maxwellian distribution, the single particle field is averaged over the velocity distribution. The electric field E in the frame of a particle moving with a velocity $\mathbf{v}$ with respect

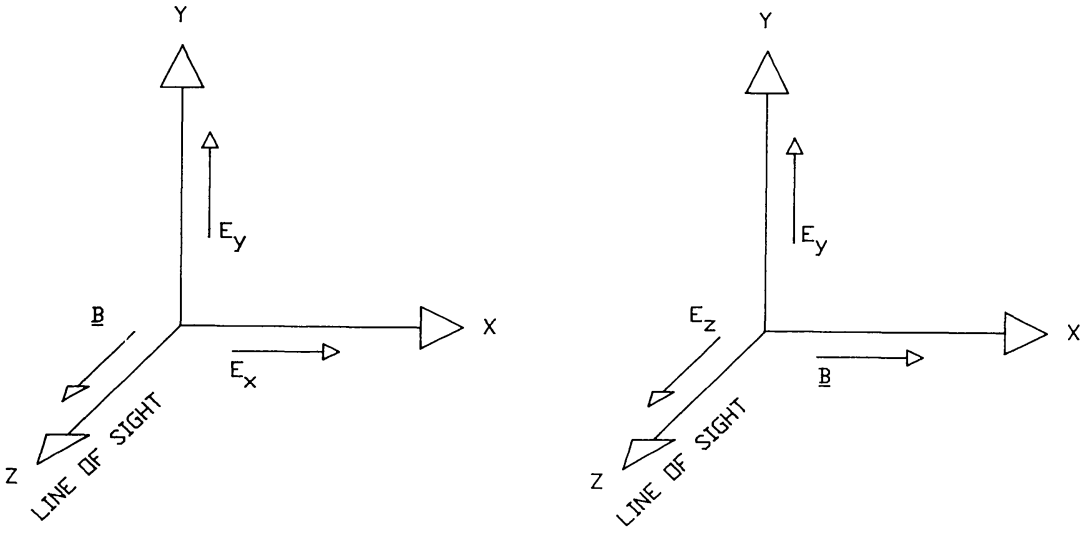

Fig. A1. Geometry of the magnetic field and motional electric field for the two cases of **B** oriented parallel to (*left panel*), and transverse to (*right panel*), the line of sight.

to a fixed frame which has an electric field $\mathbf{E}'$ and magnetic field **B** is given by

$$\mathbf{E} = \mathbf{E}' + \mathbf{v} \times \mathbf{B} \tag{A1}$$

provided $v \ll c$. Setting $\mathbf{E}' = 0$, the motional ($\mathbf{v} \times \mathbf{B}$) contribution to the electric field in the moving frame may be derived by letting **B** lie in the x, z plane ($\mathbf{B} = (B_x, 0, B_z)$) and allowing the particle velocity an arbitrary direction ($\mathbf{v} = (v_x, v_y, v_z)$). The electric field components in the moving frame are then given by

$$E_x = v_y B_z \,, \tag{A2}$$

$$E_y = v_z B_x - v_x B_z \,, \tag{A3}$$

and

$$E_z = -v_y B_x \,. \tag{A4}$$

The components of the mean electric field (absolute value) experienced by an ensemble of particles in a velocity distribution $f(\mathbf{v})$ are given by

$$\overline{E}_x = \int |E_x| \, f(\mathbf{v}) \, \mathrm{d}^3 v \,, \tag{A5}$$

$$\overline{E}_y = \int |E_y| \, f(\mathbf{v}) \, \mathrm{d}^3 v \,, \tag{A6}$$

and

$$\overline{E}_z = \int |E_z| \, f(\mathbf{v}) \, \mathrm{d}^3 v \,, \tag{A7}$$

where the integrals extend over all velocity space. Expressing the single-particle electric field in terms of the velocity and magnetic field components yields expressions for the

electric field intensities in terms of the magnetic field strengths and velocity integrals, namely

$$\overline{E}_x = |B_z| \int |v_y| \, f(\mathbf{v}) \, \mathrm{d}^3 v \,, \tag{A8}$$

$$\overline{E}_y = \int |v_z B_x - v_x B_z| \, f(\mathbf{v}) \, \mathrm{d}^3 v \,, \tag{A9}$$

and

$$\overline{E}_z = |B_x| \int |v_y| \, f(\mathbf{v}) \, \mathrm{d}^3 v \,. \tag{A10}$$

Since the velocity distribution is symmetric, the integrals in v_x, v_y, and v_z are equal. For an ensemble of hydrogen atoms in a Maxwellian distribution of temperature T, integration of the v_i (where $i = x$, y, or z) component over all velocity space yields

$$\int |v_i| \, f(\mathbf{v}) \, \mathrm{d}^2 v = 7.3 \times 10^3 \sqrt{T} \ \mathrm{cm\ s^{-1}} \,. \tag{A11}$$

The $\overline{E}_x$ and $\overline{E}_z$ calculations are straightforward, while the $\overline{E_y}$ calculation requires a separate integration for each quadrant in the v_x, v_z plane. The resulting mean absolute values of the electric field components are given by

$$\overline{E_x} = 7.3 \times 10^{-5} \sqrt{\mathrm{T}} \, |B_z| \,, \tag{A12}$$

$$\overline{E_y} = 3.7 \times 10^{-5} \sqrt{T} \, (|B_x - B_z| + |B_x + B_z|) \,, \tag{A13}$$

and

$$\overline{E}_x = 7.3 \times 10^{-5} \sqrt{T} \, |B_x| \,. \tag{A14}$$

where $\overline{E}_x$, $\overline{E}_y$, and $\overline{E}_z$ are expressed in $\mathrm{V\ cm^{-1}}$, and $|B_x|$ and $|B_z|$ are expressed in gauss.

References

Berezin, A., Dubovoi, L., and Lyublin, B.: 1972a, *Soviet Phys. Tech. Phys.* **16**, 2914.

Berezin, A., Dubovoi, L., and Lyublin, B.: 1972b, *Soviet Phys. Tech. Phys.* **17**, 750.

Bethe, H. and Salpeter, E.: 1957, *Quantum Mechanics of One- and Two-Electron Atoms*, Springer-Verlag, New York.

Dravins, D.: 1973, *Astrophys. Letters* **13**, 243.

Foukal, P. and Hinata, S.: 1991, *Solar Phys.* **132**, 307.

Foukal, P., Hoyt, C., and Gilliam, L.: 1986, *Astrophys. J.* **303**, 861.

Griem, H.: 1974, *Spectral Line Broadening by Plasmas*, Academic Press, New York.

Henze, W., Tandberg-Hanssen, E., Hagyard, M., Woodgate, B., Shine, R., Beckers, J., Bruner, M., Gurman, J., Hyder, C., and West, E.: 1982, *Solar Phys.* **81**, 231.

Hirayama, T.: 1985, *Solar Phys.* **100**, 415.

Levinton, F., Gammel, G., Kaita, R., Kugel, H., and Roberts, D.: 1990, *Rev. Sci. Instr.* **61**, 2914.

Underhill, A. and Waddell, J.: 1959, *NBS Circ.* No. 604.

White, S., Kundu, M., and Gopalswamy, N.: 1991, *Astrophys. J.* **366**, L43.

Wien, A.: 1916, *Ann. Phys.* **49**, 842.